The Frequency-Domain Transmission Line Matrix Method—A New Concept

Hang Jin, *Member, IEEE,* and Rüdiger Vahldieck, *Senior Member, IEEE*

***Abstract*—A new frequency-domain TLM method is presented for the frequency selective s-matrix computation of 3-D waveguide discontinuities. The new approach combines the flexibility of the conventional TLM method with the computational efficiency of frequency-domain methods. The basis for this new technique is a novel excitation of an impulse train of sinusoidally modulated magnitude. At any time step, this excitation retains the form of an impulse while its envelop contains the information of the structure at the modulation frequency. Utilizing the diakoptics technique in conjunction with the new concept of the intrinsic scattering matrix,which relates the reflected and incident impulses at the exterior branches of any discontinuity structure, the original electromagnetic field problem is simplified into a matrix algebra problem, allowing the use of linear algebra tools to further enhance the computational efficiency of the algorithm. A variety of structures have been analyzed in order to check the accuracy of this new approach and excellent agreement has been observed in all cases. *S*-parameters for CPW air-bridges including finite thickness and conductivity of the metallizations are computed. For the first time in literature, also the effect of superconductor air-bridges is analyzed.**

I. Introduction

THE TLM method is known as a general purpose time-domain technique suitable for the simulation of wave propagation phenomena in guided wave structures and discontinuities of arbitrary shape (i.e., [1]–[10]). In the three-dimensional TLM method, the space is discretized by a three-dimensional transmission line network in which impulses are scattered among the junctions of the transmission lines (nodes) and the boundaries at a fixed time step. Thus the problem is discretized in both time and space and the impulse distribution within the network describes the evolution of the electromagnetic field.

Although the method is very versatile and useful to provide a physical picture of the behaviour of the electromagnetic field at discontinuities of arbitary shape, it is in general less effective, compared to frequency-domain techniques, in characterizing the frequency selective response of transmission line structures. There are several reasons for this. First of all, due to the impulse excitation, the TLM algorithm involves a theoretically infinite frequency range before, through a Fourier transform, the frequency range of interest can be selected. This means much more information is processed than is actually needed in the design (or analysis). In addition, the TLM algorithm is an iterative process for solving a system of linear equations with a coefficient matrix and initial values. This procedure is naturally slow since many advance matrix algebra techniques (i.e., QR or QL techniques) cannot be applied and relatively long computer run-times are the result. Furthermore, the transformation from the time-domain into the frequency domain introduces errors which are not always negligible. The following describes some of the problems associated with this transformation.

Frequency-Domain Errors: The TLM method is subject to various sources of error, such as the finite truncation of the impulses in time or finite discretization in space and time. This leads to errors, which may be small and negligible in the time-domain, but can cause substantial errors at some frequencies in the frequency domain, because it is a well known fact that a small error in one of a pair of Fourier transforms may result in a considerable error in the other [11]. It is difficult or impossible to determine in advance at which frequencies these errors are significant. The accuracy of the field amplitude derived from this procedure and hence the ratio between incident and reflected fields (s-parameter) may therefore be inaccurate.

Multi-Mode Problem: The impulse response of the TLM network contains the entire frequency spectrum, so that in principle all the modes of the structure can be excited. After the Fourier transformation of the impulse response, the resulting field is obtained as a superposition of the modes that exist at the frequency at which the Fourier transform is performed. If the structure can support more than one mode at this frequency, the resulting field cannot be separated in fundamental and higher order modes. This is in particular a problem when open structures are simulated as discussed below.

The above mentioned problems are related to potential error sources when a time-domain method is applied to frequency selective problems. Thus, limiting the application range of the TLM method. Another limitation of the TLM method is in the treatment of open structures [12], [13]. Since the TLM method is discretizing space and time, the space must be of finite volume. To realize this in practice, the open structure is approximated by either a closed metallic (magnetic) box of appropriate size

Manuscript received March 31, 1992; revised August 7, 1992.

The authors are with the Laboratory for Lightwave Electronics, Microwaves and Communications (LLiMiC), Department of Electrical and Computer Engineering, University of Victoria, Victoria, BC V8W 3P6.

IEEE Log Number 9203685.

or absorbing boundaries. The closed metallic (magnetic) box introduces a large number of unwanted box modes which are non existent in an open structure, and can not be separated from the real modes of the structure. Although these modes can be avoided to some extent by choosing the excitation point where the field of the unwanted mode is zero, this will require the *a priori* knowledge of the field pattern, which is not always possible. The absorbing boundary on the other hand, is simulating the open space by absorbing all the incident waves in the time-domain at that boundary. Unfortunately, there are no absorbing conditions that meet the requirement of perfect absorption without increasing the computation time significantly. Practically, every absorbing boundary will produce a few percent of reflection. This may have no significant effect on the time domain solution, but may cause unacceptable errors in some frequency components [12]–[14].

In order to retain the flexibility of the TLM method and at the same time avoid the problems that occur when transforming from one domain into another, the frequency-domain TLM (FDTLM) method has been developed. In this method the space is discretized by the same transmission line network as in the conventional time-domain TLM (TDTLM). However, instead of exciting the network with a single impulse, an impulse train of sinusoidally modulated magnitude is used. At any time step, this new excitation retains the form of an impulse but its modulated envelope contains the information of the structure at a particular modulation frequency. Hence, the frequency information of the system is directly obtained from the impulse response amplitude rather than through the Fourier transformation. Since the solution procedure is essentially carried out in the frequency-domain, this new method can handle multiple mode structures and take advantage of the numerous advanced frequency-domain techniques, such as the diakoptics, to greatly enhance its computational efficiency.

This paper is organized as follows. Section II gives a detailed description of the novel excitation used in this new method. In Section III, the concept of the intrinsic scattering matrix is introduced, which along with the new excitation, builds the foundation for this new method. The algorithm of the FDTLM in the case of 2-D guiding structures is described in Section IV and for 3-D waveguide discontinuities in Section V. Numerical results are given in Section VI to validate this new approach.

II. Excitation

One of the differences between time- and frequency-domain methods is their excitation: Time-domain methods utilize impulses while frequency-domain methods employ sinusoidal waves. For example, assuming an input excitation in the TLM network at some branch at time $t = 0$, the output is an impulse sequence taken at the output branch. With respect to the input and output branches, the problem can be represented as a general two terminal network as shown in Fig. 1(a). The system response in the time-domain is then contained in the magnitude of the output impulse sequence. The output voltage at frequency ω is obtained from the Fourier transformation of the impulse response:

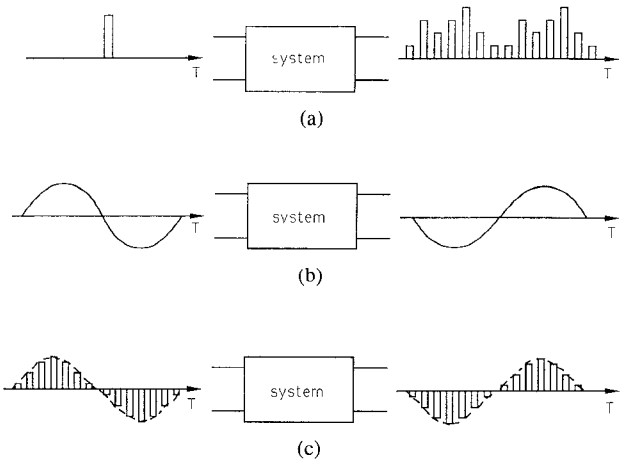

Fig. 1. Summary of three possible excitation: (a) Impulse in the time domain. (b) Sinusoidal wave in the frequency domain. (c) Impulse sequence with its magnitude modulated by a sinusoidal wave as used in the FDTLM.

$$V_{\text{out}}(\omega) = \sum_{k=1}^{\infty} v_{\text{out}}(k\Delta t) \exp(ik\omega\Delta t) \tag{1}$$

From which the transmission coefficient is obtained as

$$S_{21} = \frac{V_{\text{out}}(\omega)}{V_{\text{in}}(\omega)}. \tag{2}$$

For the same system, the frequency-domain analysis is based on a sinusoidal excitation (Fig. 1(b)). The transfer characteristics of the system at a specific frequency is contained in the amplitude of the output sinusoidal wave. Without performing a Fourier transform, the transmission coefficient, S_{21}, is directly obtained from:

$$S_{21} = \frac{V_{\text{out}}}{V_{\text{in}}} \tag{3}$$

where V_{out} and V_{in} are the amplitudes of output and input sinusoidal waves respectively.

This comparison indicates, that the same TLM network can be used in the time- as well as in the frequency-domain as long as the appropriate excitation is applied. In other words, the two types of excitation, the impulse and sinusoidal wave, can be applied simultaneously in the same TLM network. To prove this point, we employ a novel excitation in the following approach, which is not an impulse nor a sinusoidal wave but a combination of both: an impulse sequence with its magnitude modulated by a sinusoidal wave as shown in Fig. 1(c). At any time step, this new excitation retains the form of an impulse but the modulated amplitude envelope of the impulse sequence contains the information of the structure analyzed. The modulated impulse in Fig. 1(c) can also be regarded as a continuous waveform, as used in the frequency-do-

main, sampled at discrete times for observations. The advantage of considering a magnitude modulated impulse sequence, rather than a continuous sinusoidal waveform, is that the TLM time-domain algorithm still may be used in this new frequency approach whenever necessary, because at any time step the excitation retains the form of an impulse. However, due to the sinusoidal modulation frequency, the frequency-domain information is directly provided. In other words, the sinusoidal impulse excitation establishes a direct connection between the time- and frequency-domain. In the following discussion the meaning of an impulse at any time step actually means, that it is one of those impulses in the impulse sequence with its amplitude modulated by a sinusoidal wave.

III. Intrinsic Scattering Matrix

Consider a space discretized by the TLM network with N exterior branches connecting the space to the surrounding space (Fig. 2). At these exterior branches, incident impulses, with their magnitude modulated by a sinusoidal wave as described before, are injected and the reflected impulses are observed. These reflected impulses, after a sufficiently long period of time, would become a modulated impulse sequence with the same modulation frequency as the incident inpulse train. The magnitude of the reflected impulses are linearly related to that of the incident impulses, assuming that there are no nonlinear events taking place within the TLM network. Therefore, the following relationship between incident and reflected impulses holds:

$$V_e^r = M \cdot V_e^i \tag{4}$$

where V_e^i and V_e^r are the magnitudes of the incident and reflected impulses at the exterior branches. M is defined as the intrinsic scattering matrix of the structure. M is solely determined by the properties of the structure itself and the modulation frequency and can be derived from the scattering matrix S of the network and the connection matrix C. To derive the intrinsic scattering matrix M, it is first necessary to classify all the branches in the TLM network into three types: interior, exterior and stub branches. Interior branches connect the nodes within the network while exterior branches connect nodes in the network to the surrounding space. Stub branches are used to represent a dielectric. This is expressed as

$$\begin{bmatrix} {}_kV_i^r \\ {}_kV_e^r \\ {}_kV_s^r \end{bmatrix} = \begin{bmatrix} S_{11} & S_{12} & S_{13} \\ S_{21} & S_{22} & S_{23} \\ S_{31} & S_{32} & S_{33} \end{bmatrix} \cdot \begin{bmatrix} {}_kV_i^t \\ {}_kV_e^t \\ {}_kV_s^i \end{bmatrix} \tag{5}$$

where ${}_kV_i^t$, ${}_kV_e^t$ and ${}_kV_s^t$, respectively, are the incident voltage vectors of the interior, exterior and stub branches at time step k. ${}_kV_i^r$, ${}_kV_e^r$, and ${}_kV_s^r$ are the corresponding reflected voltage vectors. In the next time step $k + 1$, the reflected voltages, ${}_kV_s^r$, will become the incident voltages at the same branches:

$${}_{k+1}V_s^t = {}_kV_s^r. \tag{6}$$

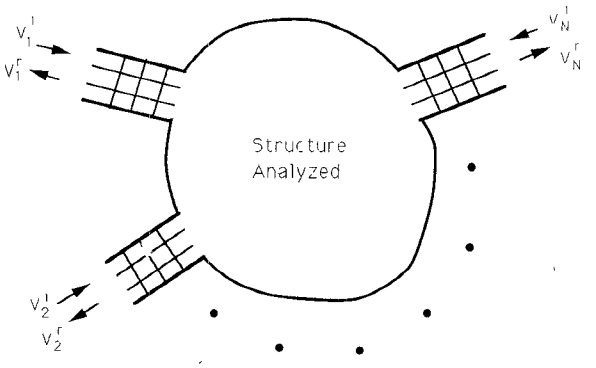

Fig. 2. Space discretized by the TLM network with N exterior branches connecting the space to the surrounding space.

For the interior branches, the incident voltages at time step $k + 1$ are the reflected voltages of the adjacent interior branches at the previous time step k. They are related through the connection matrix C:

$${}_{k+1}V_i^i = C \cdot {}_kV_i^r. \tag{7}$$

Since the magnitude of the impulses is modulated by a sinusoidal wave, the impulse amplitude at time step $k + 1$ is different from the impulse amplitude at time k by only a factor $\exp(i\omega\Delta t)$, where Δt is the time step and ω the modulation frequency. This yields

$${}_{k+1}V_s^t = \exp(i\omega\Delta t) \cdot {}_kV_s^i \tag{8a}$$

$${}_{k+1}V_i^t = \exp(i\omega\Delta t) \cdot {}_kV_i^i \tag{8b}$$

Substituting (8) into (6) and (7), one obtains

$${}_kV_s^i = \gamma \cdot {}_kV_s^r \tag{9a}$$

$${}_kV_i^t = \gamma \cdot C \cdot {}_kV_i^r \tag{9b}$$

where $\gamma = \exp(-i\omega\Delta t)$.

Therefore, from (5) and (9), a relationship can be established between ${}_kV_e^r$ and ${}_kV_e^i$:

$$\begin{aligned} {}_kV_e^r = \{&\gamma[S_{21} + \gamma S_{23} \cdot G \cdot S_{31}] \cdot C \\ &\cdot [1 - \gamma(S_{11} + \gamma S_{13} \cdot G \cdot S_{31}) \cdot C]^{-1} \\ &\cdot [S_{12} + \gamma S_{13} \cdot G \cdot S_{32}] \\ &+ S_{22} + \gamma S_{23} \cdot G \cdot S_{32}\} \cdot {}_kV_e^i \end{aligned} \tag{10}$$

where $G = (1 - \gamma S_{33})^{-1}$.

Equation (10) provides an explicit expression for the intrinsic scattering matrix M in terms of the scattering and connection matrices of the network. To simplify the equations, in the following discussion the subscript k for the time will be omitted.

Normalizing the voltages by the branch impedances

$$V = Y^{-(1/2)} \cdot v \tag{11}$$

whereby $Y^{1/2}$ is a diagonal matrix with the ith element $Y_i^{1/2}$ and Y_i being the admittance of the ith exterior branch. Substitute (11) into (10), yields

$$v^r = Y^{1/2} \cdot M \cdot Y^{-(1/2)} \cdot v^t. \tag{12}$$

The normalized intrinsic scattering matrix $m = Y^{1/2} \cdot M \cdot Y^{-(1/2)}$ is symmetrical. This can be verified by considering that the TLM network is a passive electrical network to which the reciprocity theorem [16] can be applied.

The intrinsic scattering matrix m fully characterizes the structure and plays a central role in this new approach. By establishing the intrinsic scattering matrix, the original electromagnetic problem is transformed into a matrix algebra problem. Once the intrinsic scattering matrix has been found, all the properties of the structure, such as the propagation constant Γ of the guide connecting two subsequent discontinuities, can be readily computed through matrix operations. This is the major advantage of this new approach. Transforming the electromagnetic field problem into a matrix operation problem, the vast area of numerical techniques in matrix theory is available to enhance the computational efficiency of the algorithm. Furthermore, on the basis of the intrinsic scattering matrix, the diakoptics technique can be easily implemented. By finding the intrinsic scattering matrix for each substructure, the intrinsic matrix for the entire structure can be obtained from simple matrix operations. Details of this procedure for the 2-D and the 3-D problem will be described in the following sections.

IV. 2-D Guiding Structure

For any guiding structure the intrinsic scattering matrix m is constructed from a *slice* of waveguide which contains only one node in the propagation direction (Fig. 3). For this case (12) is written as follows:

$$\begin{bmatrix} b_1 \\ b_2 \end{bmatrix} = m \cdot \begin{bmatrix} a_1 \\ a_2 \end{bmatrix} = \begin{bmatrix} m_{11} & m_{12} \\ m_{21} & m_{22} \end{bmatrix} \cdot \begin{bmatrix} a_1 \\ a_2 \end{bmatrix} \tag{13}$$

where a_1 and a_2 denote the voltage vectors and b_1 and b_2 the reflected voltage vectors. Performing the following variable transformation in (13):

$$\begin{aligned} v_1 &= (a_1 + b_1); \qquad i_1 = (a_1 - b_1) \\ v_2 &= (a_2 + b_2); \qquad i = (a_2 - b_2) \end{aligned} \tag{14}$$

leads to

$$\begin{bmatrix} v_2 \\ -i_2 \end{bmatrix} = \begin{bmatrix} A & B \\ C & D \end{bmatrix} \cdot \begin{bmatrix} v_1 \\ i_1 \end{bmatrix} \tag{15}$$

with i_1, i_2 representing the total currents, v_1 and v_2 the total voltages. The submatrices A, B, C, D can be expressed by matrices m_{11}, m_{12}, m_{21}, m_{22}:

$$\begin{aligned} A &= Z_{22} \cdot Z_{12}^{-1} \\ B &= Z_{21} - Z_{22} \cdot Z_{12}^{-1} \cdot Z_{11} \\ C &= -Z_{12}^{-1} \\ D &= Z_{12}^{-1} \cdot Z_{11} \end{aligned} \tag{16}$$

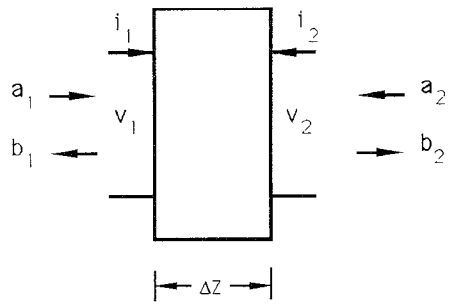

Fig. 3. A slice of waveguide with a length of Δz in z direction.

where Z_{11}, Z_{12}, Z_{21}, and Z_{22} are given as

$$\begin{bmatrix} Z_{11} & Z_{12} \\ Z_{21} & Z_{22} \end{bmatrix} = [1 - m]^{-1} \cdot [1 + m]. \tag{17}$$

It is found that matrices A, B, C, D are related in the following way [17]:

$$\begin{aligned} A \cdot B &= B \cdot D \\ C \cdot A &= D \cdot C \\ B \cdot C &= A \cdot A - 1 \end{aligned} \tag{18}$$

Considering that the entire guiding structure can be viewed as a cascaded composition of many equal *slices*, then, according to the definition for propagating modes, the voltage v_2 and current $-i_2$ differ from v_1 and i_1 by only a constant factor $\exp(-\Gamma \Delta z)$. Where Δz is the size parameter, i.e., the length or thickness of each slice in the propagation direction and Γ is the propagation constant to be determined. Equation (15) can be rewritten as:

$$\exp(-\Gamma \Delta z) \cdot \begin{bmatrix} v_1 \\ i_1 \end{bmatrix} = \begin{bmatrix} A & B \\ C & D \end{bmatrix} \cdot \begin{bmatrix} v_1 \\ i_1 \end{bmatrix} \tag{19}$$

or rewriting (19):

$$B \cdot i_1 = [e^{-\Gamma \Delta z} - A] \cdot v_1 \tag{20}$$

$$(1 - e^{\Gamma \Delta z} \cdot D) \cdot i_1 = e^{\Gamma \Delta z} \cdot C \cdot v_1 \tag{21}$$

and multiplying (21) by B and using (18), yields

$$(1 - e^{\Gamma \Delta z} \cdot A) \cdot B \cdot i_1 = e^{\Gamma \Delta z} \cdot (A \cdot A - 1) \cdot v_1. \tag{22}$$

Substituting (20) into (21) and simplifying leads to

$$\cosh(\Gamma \Delta z) \cdot v_1 = A \cdot v_1 \tag{23}$$

Equation (23) is the standard form of an eigenvalue problem, which can be solved, for example, by the QR factorization method. Notice that the eigenvalue factor $\cosh(\Gamma \Delta z)$ in (23) is an even function of Γ, meaning that each eigenvalue of (23) leads to a pair of Γ with the same magnitude but opposite sign. This corresponds to the positive or negative propagation direction of the modes.

After the eigenvalue Γ and its corresponding eigenvector v_1 are found from (23), the current i_1 can be found

from (20). The most convenient form for i_1 can be obtained by repeating the same derivation from (20) to (23) but eliminating v_1:

$$\cosh(\Gamma\Delta z) \cdot i_1 = D \cdot i_1 \tag{24}$$

Substitute (24) into (21), we find:

$$i_1 = -\sec h^{-1}(\Gamma\Delta z) \cdot C \cdot v_1. \tag{25}$$

Finally, the incident and reflected impulses a_1 and b_1 can be obtained from (14).

V. 3-D Discontinuity

A 3-D discontinuity can always be divided into two areas: the region containing the discontinuity and the transmission line structures attached to the discontinuity as the input and output ports. The calculation of the scattering parameters for the 3-D discontinuity with the FDTLM involves the following steps. First the intrinsic scattering matrices for the discontinuity region and the transmission lines attached to it are determined. Then the 2-D analysis is performed for the connected transmission lines to find the field distribution for the propagating modes. One of the ports is then excited by its modal field. From the reflected and the transmitted field amplitudes the scattering parameters can be found. In the following, details of this procedure are given for a two-port discontinuity problem.

The two-port structure in Fig. 4 may be broken up into three sub-structures: the discontinuity region and the two semi-infinity waveguides attached as input and output ports. First the intrinsic scattering matrices for each of these sub-structures are to be determined. The intrinsic scattering matrix for the discontinuity region can be readily obtained from its scattering matrix and connection matrix as shown in (10). However, for the semi-infinite waveguides, the calculation of the intrinsic scattering matrices is more involved. The general calculation procedure and the mathematical expressions presented in the previous sections can not be applied directly in this case, since the space involved is infinitely extended in z-direction. In this case, the exterior branches are located in the cross-section of the waveguide pointing in propagation direction and the incident and reflected impulses at these exterior branches are related by the intrinsic scattering matrix. To distinguish this case from the general case of scattering in all directions, the intrinsic scattering matrix will be referred to as the reflection matrix R of the semi-infinite waveguide.

Matrix R can be constructed from the modes of the waveguide by taking a slice of the guide and then finding its intrinsic scattering matrix M. As described in the previous section, all the modes of the waveguide can be obtained from M. Assuming there are N pairs of solutions and a_i, b_i $(i = 1, 2, \cdots, N)$ are the incident and reflected impulses of the modes, which propagate along the positive z-axis, then an arbitrary wave can be expanded as

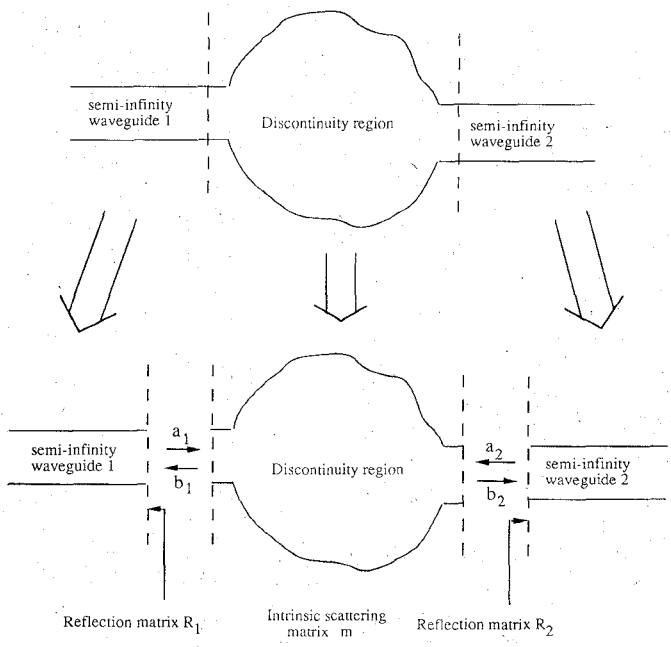

Fig. 4. Subdivision of a two-port waveguide discontinuity.

$$a = \sum_{i=1}^{N} A_i a_i \tag{26}$$

$$b = \sum_{i=1}^{N} A_i b_i \tag{27}$$

where a and b are the incident and reflected impulses of this wave. In matrix notation, this equation reads as

$$a = [a_i] \cdot [A] \tag{28}$$

$$b = [b_i] \cdot [A] \tag{29}$$

where $[a_i]$ and $[b_i]$ are the matrices with the ith column being the vector a_i and b_i, respectively. $[A]$ is the vector containing all the coefficients A_i. Eliminating $[A]$ in (28) and (29), establishes the relationship between a and b:

$$b = [b_i] \cdot [a_i]^{-1} \cdot a. \tag{30}$$

Thus, the reflection coefficient matrix R for a semi-infinity waveguide is given by:

$$R = [b_i] \cdot [a_i]^{-1}. \tag{31}$$

After the intrinsic scattering matrix of the discontinuity region and the reflection matrices of the two semi-infinity waveguides are found, the problem is reduced to a matrix algebra problem as illustrated in Fig. 4. In the discontinuity region, a_1 and a_2 are the incident impulses while b_1 and b_2 are the reflected impulses. Both are related by:

$$\begin{aligned} b_1 &= m_{11} \cdot a_1 + m_{12} \cdot a_2 \\ b_2 &= m_{21} \cdot a_1 + m_{22} \cdot a_2. \end{aligned} \tag{32}$$

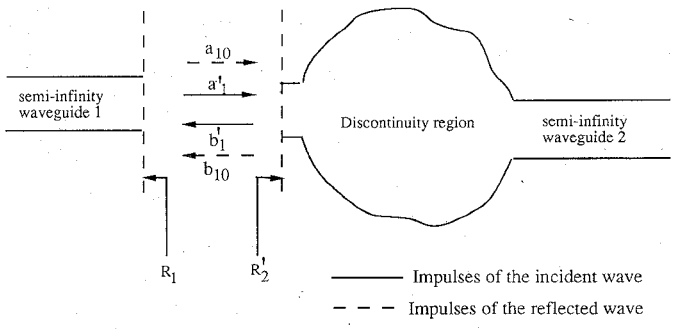

Fig. 5. Equivalent structure for a two-port waveguide discontinuity.

For port 2, b_2 is the incident impulse while a_2 is the reflected impulse, hence:

$$a_2 = R_2 \cdot b_2. \tag{33}$$

Thus, from (32) and (33), the following relationship is obtained:

$$b_1 = R_2' \cdot a_1 \tag{34}$$

$$b_2 = T' \cdot a_1 \tag{35}$$

where T' and R_2' are given by

$$R_2' = m_{11} + m_{12} \cdot R_2 \cdot T' \tag{36}$$

$$T' = (1 - m_{22} \cdot R_2)^{-1} \cdot m_{21}. \tag{37}$$

This shows that the problem has now been simplified to a one-port as illustrated in Fig. 5. The reflection coefficient R_2' contains the total effects of the discontinuity region as well as the characteristics of port 2. Assuming the excitation is incident at port 1, then the total wave a_1 and b_1 is the sum of two parts:

$$a_1 = a_{10} + a_1' \tag{38}$$

$$b_1 = b_{10} + b_1' \tag{39}$$

where a_{10}, b_{10} are the initial incident waves (excitation) and a_1', b_1', are the reflected waves. a_{10} is related to b_{10} by

$$b_{10} = R_1 \cdot a_{10}. \tag{40}$$

For the reflected waves a_1', and b_1', the propagation direction is in the negative z-axis. Therefore, in this case the reflected wave b_1' will become the incident impulse and a_1' the reflected impulse. Both are also related by the reflection matrix R_1:

$$a_1' = R_1 \cdot b_1' \tag{41}$$

b_1' is then calculated from (34), (38), and (41)

$$b_1' = (1 - R_2' \cdot -R_1)^{-1} \cdot (R_2' - R_1) \cdot a_{10}. \tag{42}$$

The total transmitted wave is calculated from (35):

$$b_2 = T' \cdot a_1 = T' \cdot (R_1 \cdot b_1' + a_{10}) \tag{43}$$

$$a_2 = R_2 \cdot b_2. \tag{44}$$

The reflected and transmitted waves given by (41)–(44), are the total fields containing all the modes of the corresponding waveguides. The field components of a specific mode can be extracted by use of (28) or (29), that is

$$[A] = [a_i]^{-1} \cdot a \tag{45}$$

or

$$[A] = [b_i]^{-1} \cdot b \tag{46}$$

where a and b are the total fields given by (41)–(44). Normalizing the modal field a_i and b_i such that the complex power carried in each of the modes equals 1, the scattering parameters for the first mode at port 1 and port 2 will be

$$s_{11} = A_1^r, \quad s_{21} = A_1^t \tag{47}$$

A_1^r and A_1^t are the first elements of (45) with a substituted by the element of the total reflected and transmitted wave.

VI. Numerical Results

To validate the accuracy of the results obtained from this new approach, a variety of different structures are calculated and compared with data from other numerical techniques. The reference planes for the scattering parameters are located in the 3-D discontinuity plane, because this new approach can take into account all the modes excited at the discontinuity. This is an additional advantageous feature of this method. It allows to minimize the volume of the space to be discretized and therefore reduces the required computer resources. The phase delay due to the propagation among the nodes is fully taken into account in the algorithm as indicated in (8). The layout of the mesh and its size is only limited by the spatial field resolution. The hybrid symmetric condensed node with non-uniformed mesh layout is used throughout the following analysis.

The diakoptics technique has been implemented in the algorithm to enhance the computational efficiency. For this the entire structure is broken up into sub-structures which are characterized independently and then cascaded with the other sub-structures. Consider a structure which is broken up into two sub-structures, 1 and 2. For sub-structure 1, (12) is rewritten as follows:

$$\begin{bmatrix} v_{1a}^r \\ v_1^r \end{bmatrix} = \begin{bmatrix} s_{11}^1 & s_{12}^1 \\ s_{21}^1 & s_{22}^1 \end{bmatrix} \cdot \begin{bmatrix} v_{1a}^i \\ v_1^i \end{bmatrix} \tag{48}$$

where v_{1a}^i, v_{1a}^r are the incident and reflected impulses at the branches connecting sub-structure 1 and 2, while v_1^i and v_1^r are the incident and reflected impulses at other exterior branches of the sub-structure 1. Similarly for sub-structure 2:

$$\begin{bmatrix} v_{2a}^r \\ v_2^r \end{bmatrix} = \begin{bmatrix} s_{11}^2 & s_{12}^2 \\ s_{21}^2 & s_{22}^2 \end{bmatrix} \cdot \begin{bmatrix} v_{2a}^i \\ v_2^i \end{bmatrix} \tag{49}$$

where v_{2a}^i and v_{2a}^r are the incident and reflected impulses at the branches connecting sub-structure 1 and 2, while v_2^i and v_2^r are the incident and reflected impulses at the exterior branches of sub-structure 2. Apparently, the in-

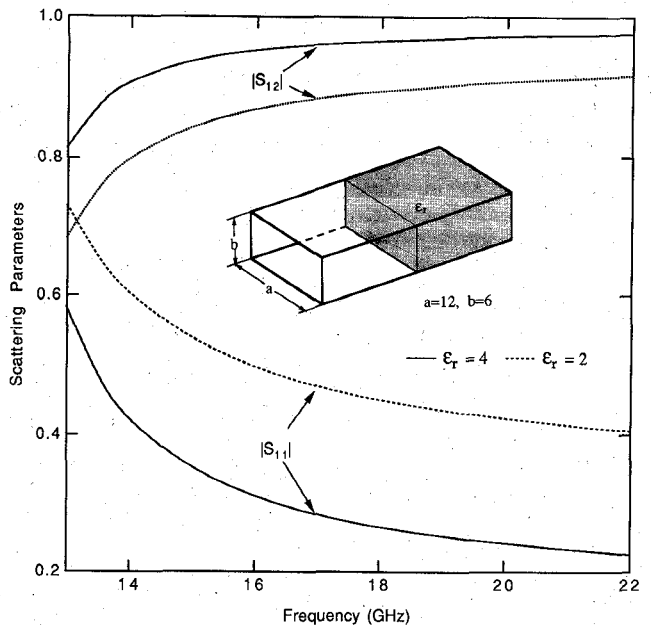

Fig. 6. Frequency-dependent S-parameters of the step junction of two dielectrics in a rectangular waveguide. The FDTLM results agree perfectly with the analytical solutions.

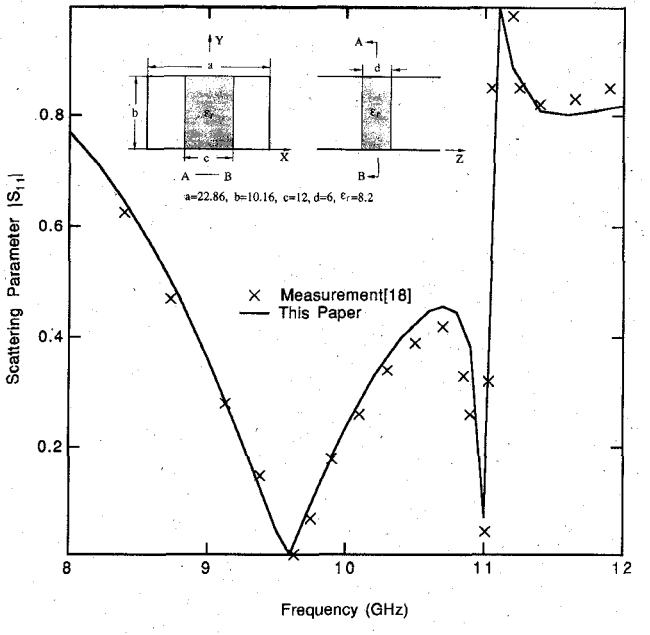

Fig. 7. The reflection coefficient for a dielectric slab of finite length in a rectangular waveguide.

cident impulses for sub-structure 1 at the connection branches are the reflected impulses for sub-structure 2 and vice versus:

$$v_{1a}^{i} = v_{2a}^{r}, \quad v_{1a}^{r} = v_{2a}^{i} \tag{50}$$

From (48)–(50) the intrinsic scattering matrix for the entire structure is obtained:

$$\begin{bmatrix} v_1^r \\ v_2^r \end{bmatrix} = \begin{bmatrix} s_{11} & s_{12} \\ s_{21} & s_{22} \end{bmatrix} \cdot \begin{bmatrix} v_1^i \\ v_2^i \end{bmatrix} \tag{51}$$

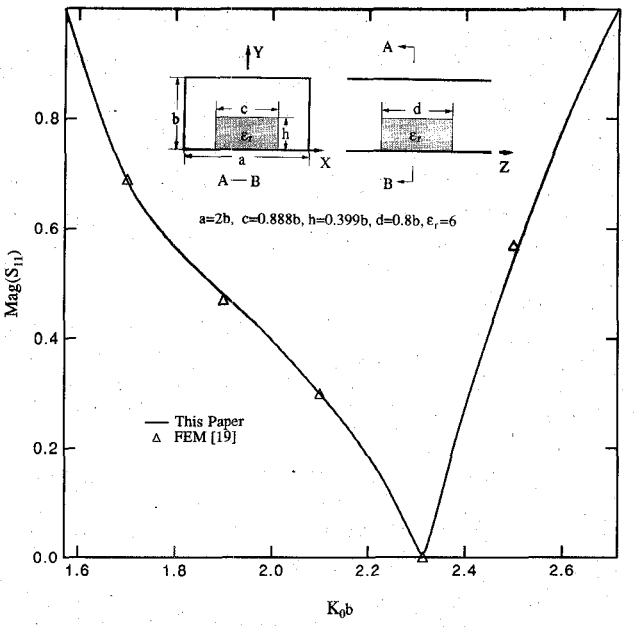

Fig. 8. The reflection coefficient for a dielectric block of finite length in a rectangular waveguide.

where:

$$\begin{aligned} s_{11} &= s_{22}^1 + s_{21}^1 \cdot (1 - s_{11}^2 \cdot s_{11}^1)^{-1} \cdot s_{11}^2 \cdot s_{12}^1 \\ s_{12} &= s_{21}^1 \cdot (1 - s_{11}^2 \cdot s_{11}^1)^{-1} \cdot s_{12}^2 \\ s_{21} &= s_{21}^2 \cdot (1 - s_{11}^1 \cdot s_{11}^2)^{-1} \cdot s_{12}^1 \\ s_{22} &= s_{22}^2 + s_{21}^2 \cdot (1 - s_{11}^1 \cdot s_{11}^2)^{-1} \cdot s_{11}^1 \cdot s_{12}^2. \end{aligned} \tag{52}$$

The first round of calculations is made for the scattering parameters of the step junction of two dielectrics in a rectangular waveguide. In this case the exact analytical solutions are available from

$$\begin{aligned} s_{11} &= \frac{Z_2 - Z_1}{Z_2 + Z_1}, \quad s_{12} = \frac{2\sqrt{Z_2 Z_1}}{Z_2 + Z_1} \\ s_{21} &= s_{12}, \qquad s_{22} = -s_{11}. \end{aligned} \tag{53}$$

Z_1 and Z_2 in (53) are the characteristic impedances of the two waveguides. The conservation of energy requires

$$|s_{11}|^2 + RE\left\{(s_{11}^* - s_{11})\sqrt{\frac{Z_1}{Z_1^*}}\right\} + |s_{12}|^2 RE\sqrt{\frac{Z_2}{Z_2^*}} = 1. \tag{54}$$

For a lossless medium, the criteria above is simplified to

$$|s_{11}|^2 + |s_{12}|^2 = 1 \tag{55}$$

The results in Fig. 6 have been checked to satisfy (55), which was always within 0.1%. Fig. 6 illustrates the perfect agreement between analytical results and the FDTLM simulation.

More complicated structures are analyzed in Figs. 7 and 8. The reflection coefficient S11 is calculated for a di-

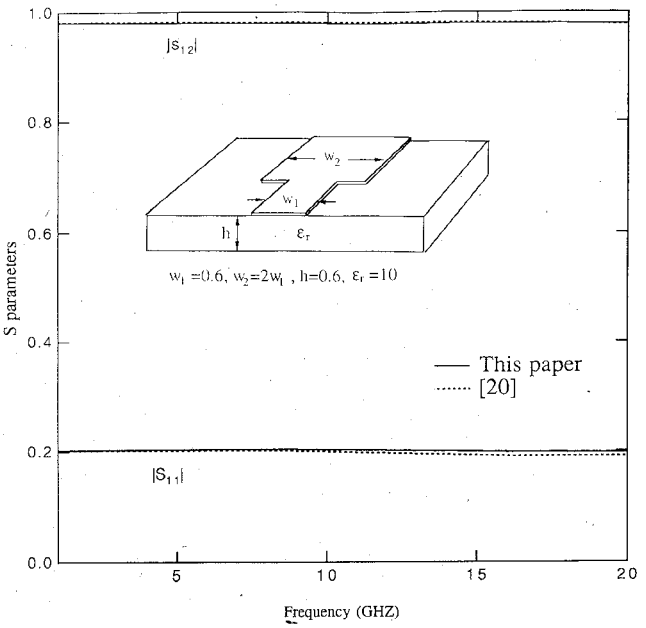

Fig. 9. Frequency-dependent S-parameters of the microstrip step-in-width.

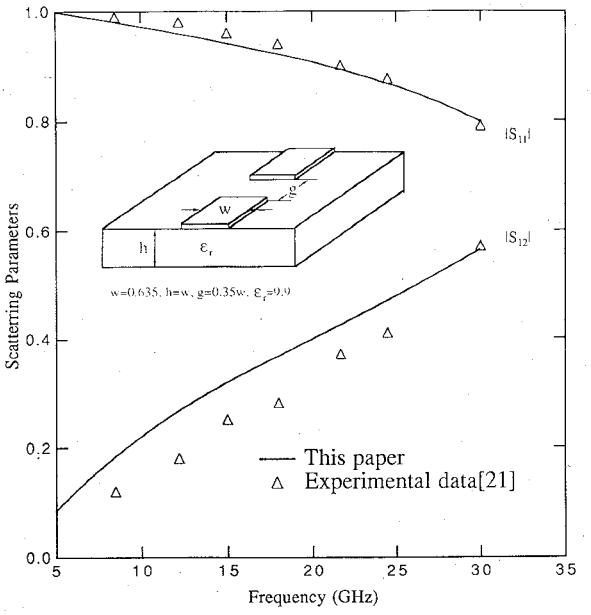

Fig. 11. Frequency-dependent S-parameters for a microstrip gap discontinuity.

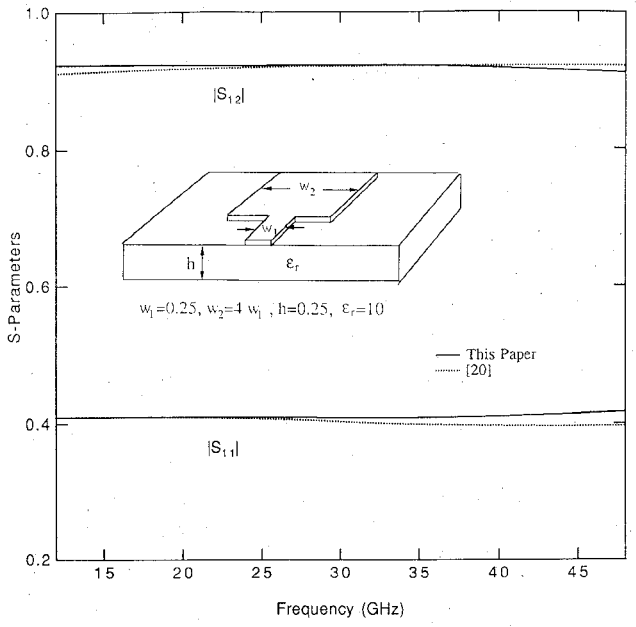

Fig. 10. Frequency-dependent S-parameters of the microstrip step-in-width.

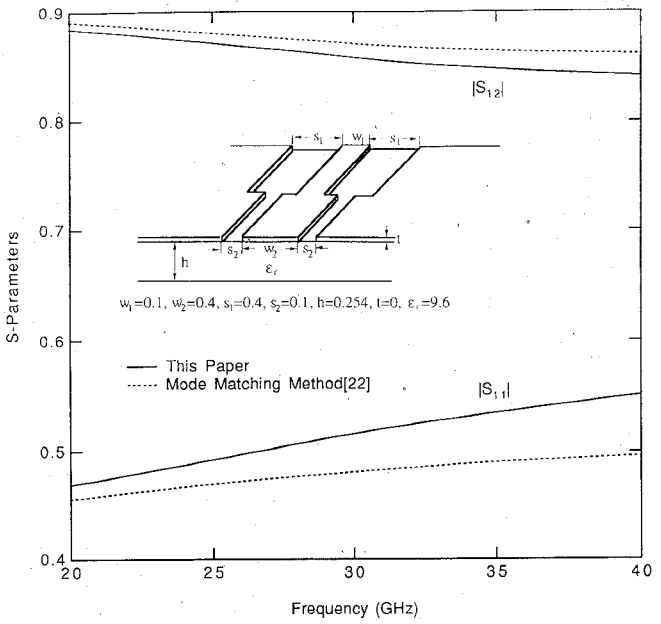

Fig. 12. Frequency-dependent S-parameters of the CPW step-in-width.

electric slab loaded waveguide of finite length in Fig. 7 and for a dielectric block of finite length in Fig. 8. In both cases, the TLM results are in excellent agreement with other methods and measurements [18], [19]. The typical computation time on a SUN SPARC II station in these cases is less than a second per frequency sample. Figs. 9 and 10 show calculated S-parameters for the microstrip step discontinuity with $w_1/H = 1.0$, $w_2/w_1 = 2.0$ and $w_1/H = 1.0$, $w_2/w_1 = 4.0$, respectively. The strip thickness is assumed to be zero and the dielectric constant is $\epsilon_r = 10$. The results are quite flat over a large frequency range and again in good agreement with the results of Koster and Jansen [20]. The typical computation time in this case is approximately 20 seconds for one frequency sample point. Fig. 11 shows the calculated S-parameters for the microstrip gap discontinuity. Also here the FDTLM results are in good agreement with measurements [21].

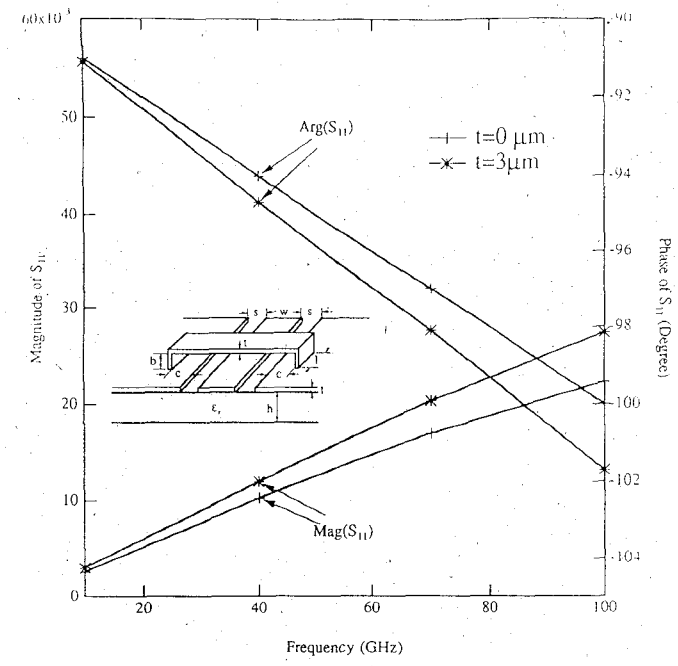

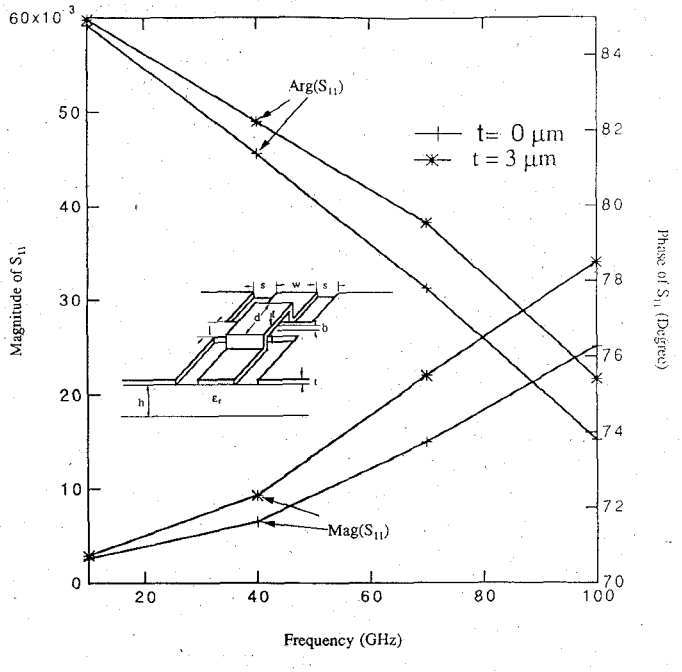

Fig. 13. Frequency-dependent reflection coefficients for CPW airbridges with two different metallization thickness $t = 0$ and $t = 3$ μm ($w = 15$ μm, $s = 10$ μm, $b = 3$ μm, $l = 30$ μm, $d = 45$ μm, $c = 0$, $h = 100$ μm, $\epsilon_r = 12.9$).

In Fig. 12 a CPW double step discontinuity is analyzed and compared with simulation results from [22]. In this case, the reference planes of the two transmission lines which connect through the discontinuity are located within the discontinuity plane. The symmetry of the structure is utilized and an artificial magnetic wall is placed at the center of the structure. Therefore, only half of the structure is simulated. The number of nodes in the x-axis is

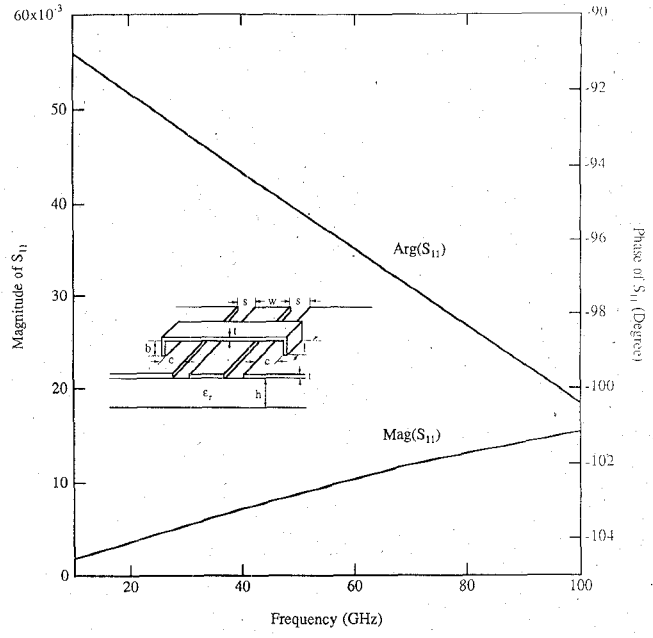

Fig. 14. Frequency dependent reflection coefficients for a superconducting CPW airbridge (YBCO: $T_c = 92.5$ K, $T = 77$ K, $\sigma_n = 1700$ s/mm, $l = 0.3$ nm, $w = 15$ μm, $s = 10$ μm, $b = 3$ μm, $l = 30$ μm, $c = 0$, $h = 100$ μm, $t = 3$ μm, $\epsilon_r = 12.9$).

chosen as 8 and the number of nodes in y-axis as 7. Increasing the number of nodes from 8 × 7 to 10 × 7 only changes the results by less than 2 percent. There are slight differences towards higher frequencies which can be reduced by increasing the number of nodes. But there is also a possibility that, due to the relative convergence problem in the mode matching method used in [22] those results are a few percent off.

The flexibility of the FDTLM method is further demonstrated by calculating the S-parameters for CPW airbridges. There are basically two types of airbridges used: The more common type is the one which bridges over the center conductor and connects both groundplane (Type A); the less frequently used airbridge bridges over the groundplane and connects the centerconductor (Type B). Fig. 13 shows a comparison between the S_{11} of both types of airbridges with different metallization thickness, $t = 0$ and $t = 3$ mm. First of all it was found, that the finite metallization thickness has only a marginal effect on the airbridge reflection coefficient. Secondly, the type B airbridge reacts slightly more sensitive to variation in the metallization thickness. This result is not surprising since the airbridge behaves basically as a parasitic capacitor connecting in parallel with the main transmission line. One part of the capacitance comes from the parallel plane capacitor between the bottom plane of the airbridge and the top plane of the center conductor. This part is almost independent from the thickness of the metallization. The other part results from the fringing fields at the ends of the air bridge and the gap of the CPW. This part of the

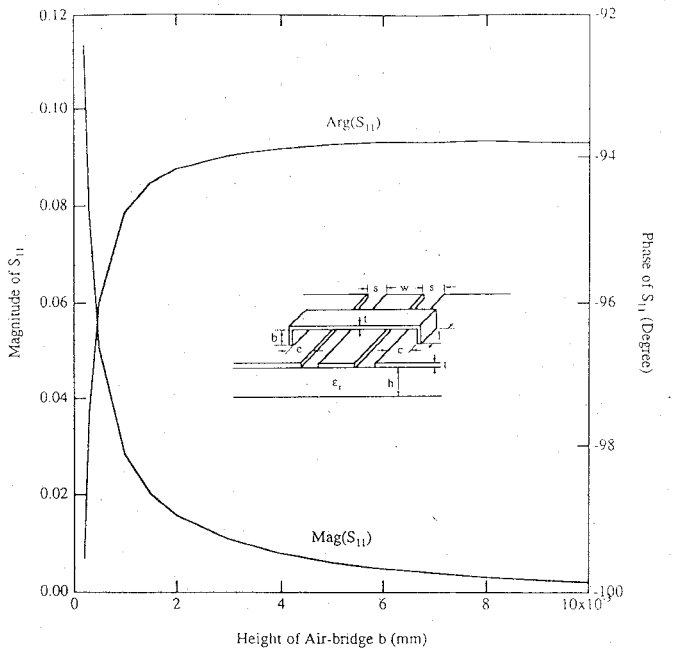

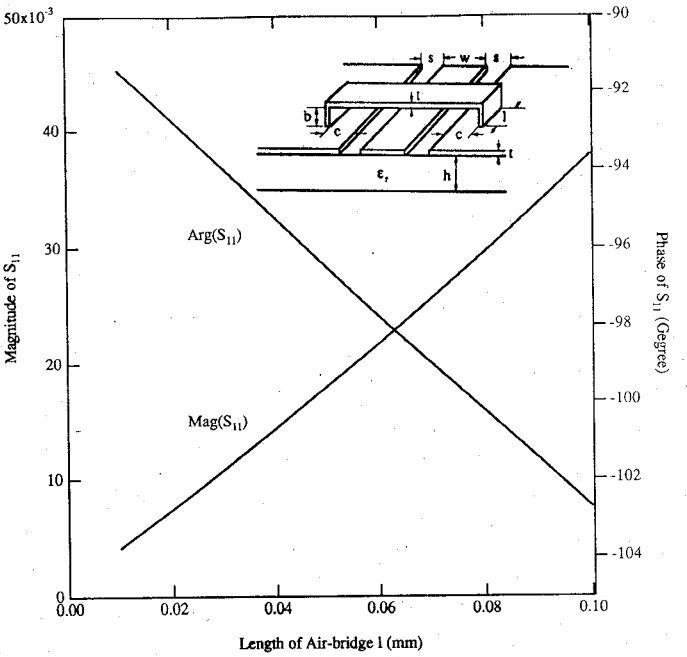

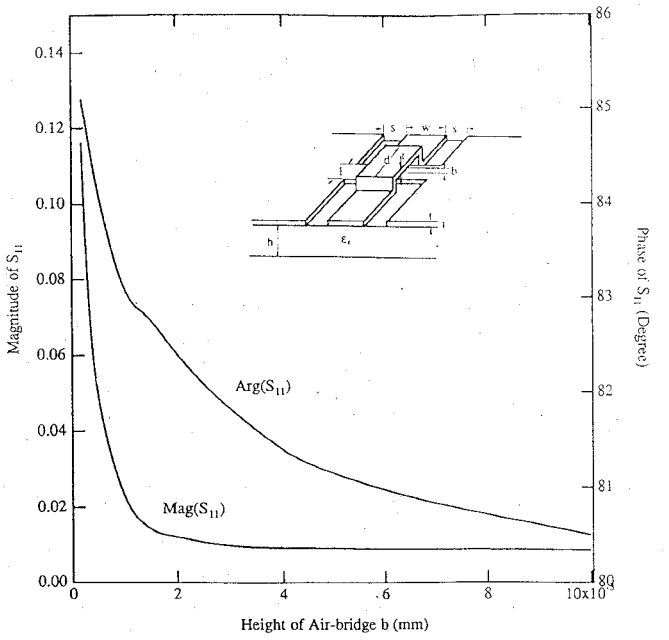

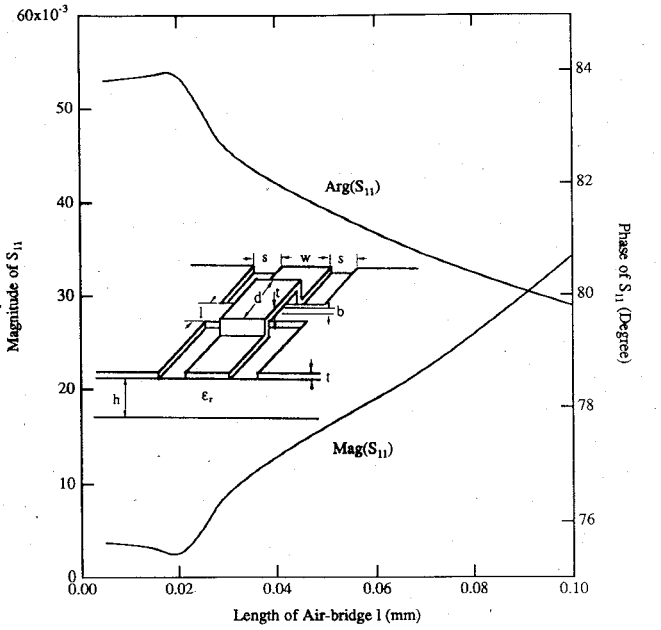

Fig. 15. Reflection coefficients for CPW airbridges versus the height of the airbridges at frequency 40 GHz (w = 15 μm, s = 10 μm, l = 30 μm, d = 45 μm, c = 0, h = 100 μm, t = 3 μm, ϵ_r = 12.9).

Fig. 16. Reflection coefficients for CPW airbridges versus the length of the airbridges at frequency 40 GHz (w = 15 μm, s = 10 μm, b = 3 μm, d = 1 + 15 μm, c = 0, h = 100 μm, t = 3 μm, ϵ_r = 12.9).

capacitance will increase with the metallization thickness, but plays only a minor role.

High-T_c superconductors are of increasing interest to reduce losses in miniaturized transmission lines. In the following we investigate the effect of superconducting airbridges on the CPW transmission characteristics. Superconductors can be incorporated in the calculations via the two-fluid model, in which a superconductor is described as a dielectric medium with the complex conductivity [23]:

$$\sigma_{\text{super}} = \sigma_n(T/T_c)^4 - j(1 - (T/T_c)^4)/\omega\mu\lambda_0^2 \quad \text{for } T < T_c \tag{56}$$

where σ_n is the normal conductivity, T is the absolute temperature, and λ_0 is the zero-temperature penetration depth. Fig. 14 shows the reflection coefficients for a superconductor airbridge. In comparison to normal conductor con-

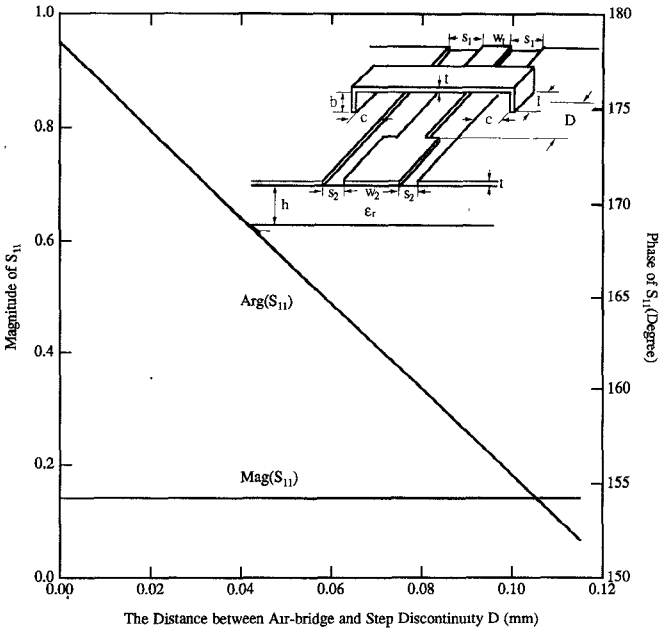

Fig. 17. Reflection coefficients for a combination of CPW airbridges and step discontinuity versus the distance between airbridge and step discontinuity at frequency 40 GHz (w_1 = 12 μm, w_2 = 20 μm, s_1 = 12 μm, s_2 = 8 μm, l = 30 μm, b = 3 μm, c = 0, h = 100 μm, t = 3 μm, ϵ_r = 12.9).

ductivities, the effect of superconductors on the S-parameters is quite small and the differences between the results of superconductors and perfect conductors are negligible.

Figs. 15 and 16 illustrate the effect of airbridge height and length on S_{11}. Both parameters seem to have an opposite effect on the phase in the different airbridges, while the tendency on $|S_{11}|$ is the same. Finally, Fig. 17 demonstrates that there is very little interaction between the location of a CPW discontinuity relative to the position of an airbirdge of type A. The change in the phase is due to the change in the length of the transmission line between both discontinuities.

VII. Conclusions

This paper has presented a new frequency-domain TLM method which operates in the frequency-domain while using the same transmission line network as the conventional TLM method. The novel sinusoidal impulse train excitation retains the form of an impulse at any time step, while the envelop of the impulse sequence contains the information of the structure. This allows to transform the conventional TLM solution procedure directly into the frequency-domain. Then frequency-domain techniques, such as the diakoptics technique, can be easily implemented in this new algorithm to enhance its computational efficiency. To improve the computational efficiency of this method even further, another new concept, the intrinsic scattering matrix, is introduced. This matrix relates the reflected and incident impulses at the exterior branches of the structure and translates the originally electromagnetic field problem into a matrix algebra problem, to which linear algebra theory can be readily applied.

A variety of structures have been analyzed in order to check the accuracy of the new method and excellent agreement has been observed in most cases. For the first time in literature, superconductor airbridges have been investigated.

References

[1] P. B. Johns and R. L. Beurle, "Numerical solution of 2-dimensional scattering problems using a transmission-line matrix," *Proc. Inst. Elec. Eng.*, vol. 118, no. 9, pp. 1203-1208, Sept. 1971.

[2] P. Saguet and E. Pic, "Un traitement du signal simple four ameliorer la methode T.L.M.," *Electron. Lett.*, vol. 16, pp. 247-248, Mar. 1980.

[3] P. Saguet and E. Pic, "Le maillage rectangulaire et le changement de maillie dans la method TLM en deux dimensions," *Electron. Lett.*, vol. 17, pp. 277-279, Apr. 1981.

[4] P. Johns, "A symmetrical condensed node for the TLM method," *IEEE Trans. Microwave Theory Tech.*, vol. MTT-35, pp. 370-377, Apr. 1987.

[5] R. H. Voelker and R. J. Lomax, "A finite-difference transmission line matrix method incorporating a nonlinear device model," *IEEE Trans. Microwave Theory Tech.*, vol. 38, pp. 302-321, Mar. 1990.

[6] P. Naylor and R. A. Desai, "New three dimensional symmetrical condensed lossy node for solution of electromagnetic wave problems by TLM," *Electron. Lett.*, vol. 26, pp. 492-494, Mar. 1990.

[7] F. J. German, G. K. Gothard, and L. S. Riggs, "Modelling of materials with electric and magnetic losses with the symmetrical condensed TLM method," *Electron. Lett.*, vol. 26, pp. 1307-1308, Aug. 1990.

[8] W. J. R. Hoefer, "The transmission-line matrix method—Theory and application," *IEEE Trans. Microwave Theory Tech.*, vol. MTT-33, pp. 882-893, Oct. 1985.

[9] W. J. R. Hoefer, "The transmission line matrix (TLM) method," in *Numerical Techniques for Microwave and Millimeter-wave Passive Structure*, Tatsuo Itoh, Ed., New York: Wiley, 1989.

[10] P. P. M. So, Eswarappa and W. J. R. Hoefer, "A two-dimensional transmission line matrix microwave field simulator using a new concepts and procedures," *IEEE Trans. Microwave Theory Tech.*, vol. 37, pp. 1877-1884, Oct. 1989.

[11] J. S. Walker, *Fourier Analysis*. New York: Oxford University Press, 1988, ch. 6.

[12] N. R. S. Simons and E. Bridges, "Method for modelling free space boundaries in TLM simulations," *Electron. Lett.*, vol. 26, pp. 453-455, Mar. 1990.

[13] N. R. S. Simons, "Application of the transmission line matrix method for open region field problems," M.Sc. thesis, University of Manitoba, 1989.

[14] X. Zhang and K. K. Mei, "Time-domain finite difference approach to the calculation of the frequency-dependent characteristics of microstrip discontinuities," *IEEE Trans. Microwave Theory Tech.*, vol. 36, pp. 1775-1787, Dec., 1988.

[15] L. A. Hageman and D. M. Young, *Applied Iteration Methods*. New York: Academic Press, 1981, ch. 2.

[16] S. Ramo, J. R. Whinnery, and T. V. Duzer, *Fields and Waves in Communication Electronics*, 2nd ed. New York: Wiley, 1984.

[17] J. Brown, "Propagation in coupled transmission line systems," *Quart. J. Mech. and Applied Math.*, vol. XI, pt. 2, pp. 235-243, 1958.

[18] H. Chaloupka, "A coupled-line model for the scattering by dielectric and ferrimagnetic obstacles in waveguides," *Arch. Elek. Ubertragung*, vol. 34, pp. 145-151, Apr. 1980.

[19] K. Ise, K. Inoue, and M. Koshiba, "Three-dimensional finite-element solution of dielectric scattering obstacles in a rectangular waveguide," *IEEE Trans. Microwave Theory Tech.*, vol. 38, pp. 1352-1359, Sept. 1990.

[20] N. L. Koster and R. H. Jansen, "The microstrip step discontinuity: A revised description," *IEEE Trans. Microwave Theory Tech.*, vol. MTT-34, pp. 213–223, Feb. 1986.
[21] M. Drissi, F. Hanna, and J. Citerne, "Theoretical and experimental investigations of open microstrip gap discontinuities," *Proc. European Microwave Conf.*, 1988, Stockholm.
[22] C. K. Kuo, T. Kitazawa, and T. Itoh, "Analysis of shield coplanar waveguide step discontinuity considering the finite metallization thickness effect," in *1991 IEEE MTT-S Int. Microwave Symp. Dig.*, Boston, pp. 473–475.
[23] W. Chew, A. L. Riley, D. L. Rascoe, B. D. Hunt, M. C. Foote, and T. W. Cooley, and L. J. Bajuk, "Design and performance of a high-T_c superconductor coplanar waveguide filter," *IEEE Trans. Microwave Theory Tech.*, vol. 39, 1991, pp. 1455–1461.
[24] Hang Jin and R. Vahldieck, "Full-wave analysis of guiding structures using a 2D array of 3D TLM nodes," accepted for publication in *IEEE Trans. Microwave Theory Tech.*

Hang Jin (M'91) was born in Jiangsu, China, on September 27, 1960. He received the B.Sc. degree in electrical engineering from the University of Science and Technology of China (USTC), Hefei, China, in 1982 and M.Eng. and D.Eng. degrees in electrical engineering from the University of Electronics Science and Technology of China, Chengdu, China, in 1984 and 1987, respectively.

Dr. Jin joined the Faculty at the University of Electronics Science and Technology of China in 1987 where he conducted research in the areas of electromagnetic scattering, radar absorbing material, and millimeter wave techniques. From 1989–1990, he was a postdoctoral fellow at the National Optics Institute, Quebec City, PQ, Canada.

Since October 1990, he has been a Research Associate at the University of Victoria, Victoria, BC, Canada. His current research areas include numerical methods for 3-D electromagnetic field problems, CAD of microwave/millimeter wave integrated (monolithic) circuits, and planar and quasi-planar components for MMIC and MHMIC applications.

Rüdiger Vahldieck (M'85–SM'86) received the Dipl.-Ing. and the Dr.-Ing. degrees in electrical engineering from the University of Bremen, West Germany, in 1980 and 1983, respectively.

From 1984 to 1986 he was a Research Associate at the University of Ottawa, Canada. In 1986 he joined the University of Victoria, BC, Canada, where he is now a Full-Professor in the Department of Electrical and Computer Engineering. His research interest include numerical methods to model electromagnetic fields for computer-aided design of microwave, millimeter wave and opto-electronic integrated circuits. He is interested in design aspects of passive and active planar and quasi-planar components and filters for MMIC and MHMIC applications. Recently he has been involved in research on subcarrier multiplexed lightwave systems. The emphasis of this work is on broad bandwidth electro-optic modulators and on coherent detection systems in fiber-optic communication links.

Dr. Vahldieck, together with three coauthors, received the outstanding publication award of the Institution of Electronic and Radio Engineers in 1983. He is on the editorial board of the IEEE TRANSACTIONS ON MICROWAVE THEORY AND TECHNIQUES and he has published more than 80 technical papers in the field of microwave CAD.